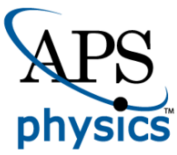

Scale-Dependent Stiffness and Internal Tension of a Model Brush Polymer

John P. Berezney, Amanda B. Marciel, Charles M. Schroeder, and Omar A. Saleh

Phys. Rev. Lett. **119**, 127801 — Published 21 September 2017

DOI: 10.1103/PhysRevLett.119.127801

Scale-dependent stiffness and internal tension of a model brush polymer

John P. Berezney
Materials Department, University of California, Santa Barbara, California 93106, USA

Amanda B. Marciel
Institute for Molecular Engineering, University of Chicago, Illinois 60637, USA

Charles M. Schroeder
Department of Chemical and Biomolecular Engineering, Center for Biophysics and Quantitative Biology, University of Illinois at Urbana-Champaign, Illinois 61801, USA

Omar A. Saleh*
Materials Department and BMSE Program, University of California, Santa Barbara, California 93106, USA
(Dated: August 23, 2017)

Bottle-brush polymers exhibit closely grafted side chains that interact by steric repulsion, thereby causing stiffening of the main polymer chain. We use single-molecule elasticity measurements of model brush polymers to quantify this effect. We find that stiffening is only significant on long length scales, with the main chain retaining flexibility on short scales. From the elasticity data, we extract an estimate of the internal tension generated by side-chain repulsion; this estimate is consistent with the predictions of blob-based scaling theories.

A brush polymer consists of a long main chain decorated along its length with short, covalently-attached side chains (Fig. 1a). This branched geometry causes brush polymers to have unique conformational behaviors that can impart particular characteristics to bulk materials. The brush geometry can be found in biological macromolecules within the extracellular matrix of tissues [1–4], and there has been recent interest in materials applications of networks of synthetic brush polymers [5].

In good solvent conditions, brush polymers are straightened by repulsive excluded-volume interactions between the side chains. This effect depends on the size of an isolated side chain (radius of gyration, R_s) relative to the grafting distance along the main chain (mb_m, where m is the average number of Kuhn monomers between grafting points, and b_m is the main-chain Kuhn length; see Fig. 1a). Brush polymer behavior can be split into two regimes based on side chain overlap [5]. In the 'comb' regime of small, well-spaced side chains, $R_s < mb_m$, the lack of side chain overlap minimizes stiffening. In contrast, brush stiffening is significant in the 'bottle-brush' regime of high grafting densities and/or large side chains, $R_s > mb_m$.

There are conflicting theoretical predictions on the nature of the stiffening effect within the bottle-brush regime [6–9], which is typically parameterized through an effective persistence length that varies with side chain size and grafting density. The issue is complicated by the chain's hierarchical structure, and the resulting scale-dependence of chain stiffness: side chain stiffening is relevant on long scales, $\gtrsim R_s$, while, on shorter scales, the main chain retains the freedom to act as a flexible random walk. The situation is reminiscent of electrostatic stiffening within polyelectrolytes, which also displays scale-dependent stiffening [10], and whose effective persistence length has also been the subject of a long-running dispute. For both bottle-brush polymers and polyelectrolytes, experiments have generally been unable to resolve the issue; this has been attributed to the complexity of scale-dependent behavior, along with differences in the manner of quantifying stiffness [11, 12].

Here, we quantify the scale-dependent stiffness of model brush polymers using single-molecule tensile elasticity measurements with a magnetic tweezer (Fig. 1b). At low applied tensions, corresponding to long length scales, we find a ten-fold stiffening of the brush complex over the main chain alone, consistent with scaling predictions [6, 9]. As the tension increases and progressively shorter length scales are probed, the effective stiffness

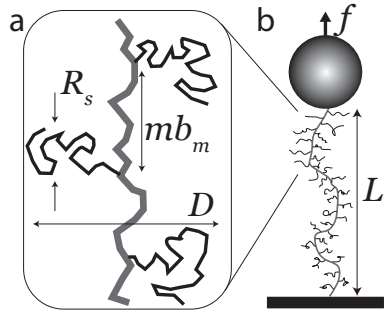

FIG. 1. (a) Sketch of brush polymer geometry: a main chain (Kuhn length b_m) is attached every m monomers to side chains of extent R_s; the resulting complex has an effective diameter D. (b) Schematic of experimental geometry: a brush polymer containing an ssDNA main chain and PEG side chains is attached to a glass surface and magnetic bead, and its length L is measured as a function of force f.

continuously decreases until it reaches the bare main-chain value. We quantify this effect through an elasticity model that combines the applied tension with an internal tension generated by side-chain repulsion, and we show that this internal tension is well-predicted by blob-based scaling theories [13].

The model brush polymers consist of a single-stranded DNA (ssDNA) main chain with poly(ethylene glycol) (PEG) side chains. The ssDNA is synthesized by a rolling circle amplification (RCA) reaction that generates chain lengths of several thousand basepairs [14], consisting of hundreds of repeats of the sequence 5′-ATGGAAAGTAAAAGAAATAAAGAAGAGT-3′ (see Fig. S1). Prior studies have found such ssDNAs to display no appreciable intramolecular base pairing [14, 15]. The RCA reaction generates relatively polydisperse ssDNA products (see Figs. S2 and S3). However, this does not affect our results: prior single-molecule measurements have established that relative elasticity, which is the focus of this work, is identical for ssDNA chains with different absolute contour lengths in the regime investigated here [21].

The RCA reaction is run either with unmodified nucleotides (to generate an unbranched control strand), or with a fraction of dibenzocyclooctyne (DBCO)-modified dUTP residues. DBCO-dUTPs replace T's in the main chain, and act as grafting points through a strain-promoted azide-alkyne cycloaddition reaction that links DBCO to azide-modified 10 kDa PEG side chains (see Fig. S1)[16, 17]. The 10 kDa mPEG azides are quite monodisperse, with polydispersity indices of 1.04 to 1.06, insuring consistent results. Grafting density is controlled by altering the ratio of DBCO-dUTP to dTTP nucleotides in the reaction mix, with a 1:4 ratio generating a sparsely-grafted chain (one side chain per 35 bases) and a 4:1 ratio generating a densely-grafted chain (one side chain per 8.75 bases).

The ssDNA is terminally labeled with thiol and biotin moieties, which are used to immobilize the complex onto a maleimide-functionalized glass flow cell, and a streptavidin-coated magnetic bead, respectively. Stretching experiments are run in a buffer containing 10 mM Tris-HCl (pH 7.5) and 30 mM NaCl, using standard magnetic tweezer force-extension protocols [18, 19]. For each candidate tethered bead, the bead height is measured as the bead is rotated to insure only a single ssDNA chain tethers the bead (if multiple tethers are present, they become interwound with rotation, leading to characteristic height changes [31]). Further, acquired data is screened for sudden changes in bead position caused by unwanted adsorption of the polymer onto the bead or glass surface; all such data are eliminated. For each type of chain, separate measurements are carried out using 1 μm diameter beads, to access low-force elasticity ($0.1 \lesssim f \lesssim 10$ pN), and 2.7 μm diameter beads, to access high force elasticity ($1 \lesssim f \lesssim 100$ pN). For comparison purposes (Fig. 2),

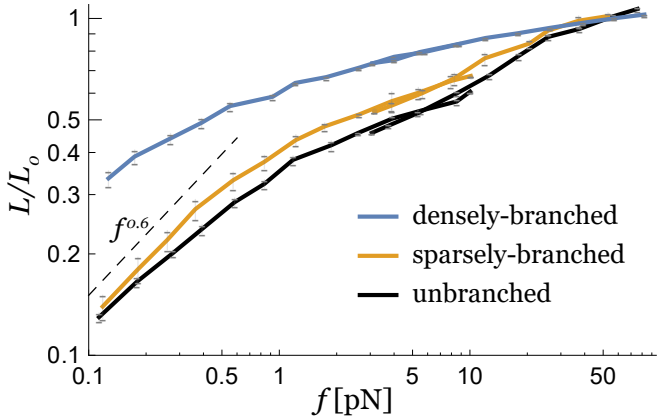

FIG. 2. Force-extension data for densely- and sparsely-branched chains, along with an unbranched control. Each curve represents binned and averaged data for 6 (unbranched), 7 (sparsely-branched) and 10 (densely-branched) separate force extension curves. Extension is normalized to the extension at 50 pN. Error bars are the SEM.

composite force-extension curves covering the full force range are generated by normalizing the high force data to unity at $f = 50$ pN, then multiplicatively adjusting the extension of the low-force data so as to minimize the sum of squared length differences between the high-force and low-force curves over the overlap regime ($1 \lesssim f \lesssim 10$ pN). For fitting (Fig. 3), the raw high-force data is used.

Given the side chain gyration radius ($R_s \approx 4.5$ nm [20]), the sparsely grafted chain ($mb_m \approx 24.5$ nm) is in the comb-polymer regime, while the densely-grafted chain is on the edge of the bottle-brush regime ($mb_m \approx 6.1$ nm). This difference has a large effect on the force-extension curves for the three polymer designs (Fig. 2). The control and sparsely-grafted chains show near-equivalent elasticity, consistent with the expectation of minimal side-chain induced effects for a comb polymer. In contrast, the densely-grafted chain maintains a longer relative extension over the entire force regime, consistent with significant side-chain repulsion leading to straightening of the complex.

By analyzing the low-force regime, we can estimate the local stiffening of the densely-grafted chain. Both the control and sparsely-grafted chains show a power-law low-force elasticity, $L \sim f^{\gamma}$, with $\gamma \approx 0.6$, consistent with the 'Pincus blob' regime of swollen-chain elasticity [21, 22]. The Pincus elastic regime terminates at a force $f_c \sim k_B T/b$, where b is the chain Kuhn length [23, 24]. For the control chain, the endpoint is $f_c \approx 1$ pN, and a relative extension ≈ 0.4, consistent with prior observations of undecorated ssDNA [21]. In contrast, no Pincus regime is observed in the densely grafted chain down to 0.1 pN. Since this lowest measured force is ten-fold lower than f_c of the control strand, we conclude that the densely-grafted chain has a Kuhn length at least ten-fold greater than the control. While this is a lower bound,

we do not expect the full stiffening to greatly exceed ten-fold: the relative extension at 0.1 pN is around 0.4, the typical transition point into Pincus elasticity. Moreover, the curve for the densely-branched polymer shows a downward curvature at 0.1 pN, which could indicate an entrance into the Pincus regime below 0.1 pN.

The stiffness of a bottle-brush polymer gives information on the side chain structure, as the molecule's Kuhn length is approximately equal to the bottle-brush diameter, D [6, 9]. Combining the ≈ 2 nm Kuhn length of undecorated ssDNA at this ionic strength [21], and the estimated ten-fold stiffening, we find the densely grafted chain has a Kuhn length and thus diameter $D \approx 20$ nm. This is a reasonable estimate of D, falling between the gyration radius (4.6 nm) and contour length (63 nm) of the side chains. Our estimate can be compared with scaling theories that predict D from models accounting for entropy loss upon side-chain stretching, the free energy of interactions between neighboring side-chains, and the entropic elasticity of the main chain. Using such an approach, Birshtein *et al.* [6] predict $D \sim b_s n^{3/5} \tau^{1/5} (n/m)^{3/25}$, where n is the number of side-chain statistical monomers, τ indicates the solvent quality, and b_s is the side-chain Kuhn length. For 10 kDa PEG in water, we estimate $n \approx 63$, $b_s \approx 1$ nm, and $\tau = 1$ (good solvent conditions), while the grafting density is $m \approx 3$. These values give $D \approx 17$ nm, in good agreement with our measurement estimate of ≈ 20 nm. We emphasize that scaling estimates are utilized three times in this discussion: first, in relating elastic regime crossover to Kuhn length, $f_c \sim kT/b$; second, in relating Kuhn length to diameter, $b \sim D$; and third, in the Birshtein scaling relation for D. For these relations, precise numerical equivalence cannot be expected.

More details on chain structure can be found from analyzing the high-force elasticity, though comparison to the ungrafted control strand is difficult: both the control and sparsely-grafted chain display an inflection point in the high-force elasticity that we attribute to mechanical unstacking of bases. Each sequence repeat of the main-chain ssDNA contains several runs of consecutive adenosines (A's). Adjacent A's have strong base-stacking interactions, forming compact, locally-helical domains of increased rigidity within an otherwise flexible, unstacked ssDNA [15, 25]. Increasing external tension leads to cooperative unstacking of those regimes, leading to a sigmoidal increase in extension at a characteristic force. The inflection point in our elastic curves occurs around 20 pN, which is consistent with values previously reported both for unstacking poly(dA) chains [15, 25], and for the specific mixed-base sequence used here [15].

In contrast, the densely-grafted chain shows a slow, monotonic increase of extension with applied force, with no apparent inflection point. This indicates that the ssDNA chain within the densely-grafted complex lacks significant stacking interactions. Yet, all ssDNA molecules in this study share the same sequence, and so might be expected to display similar unstacking behavior. We attribute the lack of unstacking in the densely-grafted chain to local disruption by the grafting itself: particularly, three of the four adenosine runs terminate at a location where a PEG-modified base can be incorporated. In the dense chain, most of these locations will indeed be occupied by a PEG-modified base. This covalent modification appears to discourage stacking.

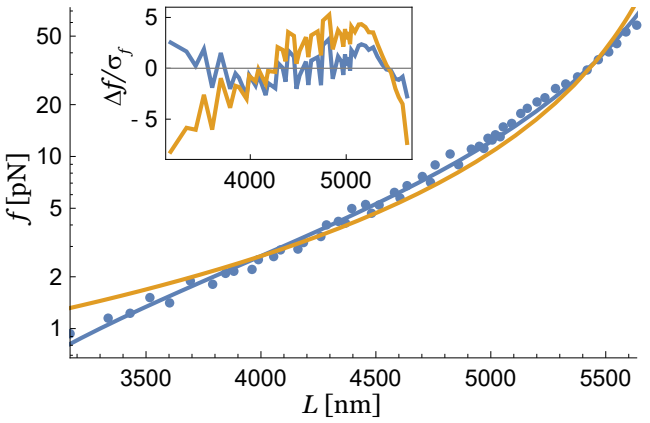

FIG. 3. Representative f versus L data for a densely-branched polymer (circles) with fits to Eq. 1 (yellow line; best-fit parameters $l_p = 3.5$ nm, $L_0 = 6000$ nm; $\bar{\chi}^2 = 11.6$) and Eq. 2 (blue line; best-fit parameters $l_p = 2.2$, $f_{int} = 1.2$ pN, $L_0 = 6150$ nm; $\bar{\chi}^2 = 2.5$). Inset: Standardized residuals, $\Delta f/\sigma_f$, vs. L for each fit. $\Delta f = f - f^*$ is the difference between data f and fit f^*, and $\sigma_f = 0.05f$ is the estimated 5% error in force.

In the absence of a pronounced enthalpic effect such as base unstacking, we expect that the densely-grafted chain displays entropic elasticity. In the high force regime, away from the crossover to swollen-chain elasticity, this can be quantitatively tested by comparison to analytical models. Here, we compare to the Marko-Siggia (MS) elasticity model for a worm-like chain (WLC) [26]. The MS-WLC model has been experimentally validated for ssDNA lacking intramolecular base pairing interactions [21, 27]; further, theoretical work predicts that WLC elasticity holds for the moderately high force range ($1 < f < 100$ pN) and chain chemistry used here [28]. We use the asymptotic form of the MS-WLC model, appropriate for large relative extensions, $L/L_0 > 0.5$ [26]:

$$L/L_0 = 1 - \sqrt{\frac{k_B T}{4 f l_p}}, \tag{1}$$

where l_p is the chain's persistence length. We apply Eq. 1 using least-squares fitting to portions of the high-force data from five separate molecules. The portions used are selected first by discarding data with $f > 63$ pN, thereby ensuring that all fitting is performed over the same range of forces for each molecule. The remaining data are subjected to a three-step fitting scheme designed to consis-

tently apply Eq. 1: i) Eq. 1 is fit to the data to determine an initial estimate of L_0; ii) this value of L_0 is used to select data with $L/L_0 > 0.5$; and iii) Eq. 1 is re-fit to the selected data. While the experiment imposed a constant applied force and measured the resulting extension, the error in force calibration ($\approx 5\%$) is significantly larger than the error in measuring length ($< 1\%$). Thus, fits are performed on transposed data, treating force as the dependent parameter and length as the independent parameter; Fig. 3 is similarly transposed with respect to Fig. 2. Least-squares fits and goodness-of-fit metrics are calculated by weighting with the 5% error in force.

Least-square fits of Eq. 1 to a representative force-extension curve are shown in Fig. 3, along with standardized residuals. Fits of the analytical MS-WLC model to all curves, along with best-fit parameters, can be found in Fig. S4 and Table S1. The fit parameters were l_p and L_0. As shown, the MS-WLC qualitatively captures the elasticity, with best-fit l_p in the range 2.6 to 4.2 nm across all 5 molecules. However, the fits quantitatively fail: clear systematic deviations can be seen in the residuals, and the reduced-chi-squared fitting metric, $\bar{\chi}^2$, ranges from 8.9 to 15.1. Note that $\bar{\chi}^2$ is normalized for the number of fit parameters, and that $\bar{\chi}^2 \approx 1$ is expected for a fit that correctly describes, but does not over-fit, the data.

We posit that the densely-grafted chains exhibit a scale-dependent stiffness, which causes Eq. 1 to fail due to its assumption of a constant l_p at all forces. To incorporate this effect, we follow recent work on charged chains [29] and use an additive-tension model: we introduce an internal tension, f_{int}, that describes the force of side-chain repulsion, and insert it into the elasticity model by replacing the applied force f with the sum of applied and internal forces, $f + f_{int}$:

$$L/L_0 = 1 - \sqrt{\frac{k_B T}{4 l_p (f + f_{int})}}. \tag{2}$$

This substitution takes inspiration from the Weiss molecular-field model for ferromagnetism [30], where susceptibility is estimated from the response of a magnetic dipole to the sum of the external field and an internal field arising from dipole-dipole interactions. Here, the additive-tension model balances the main chain entropic elasticity (parameterized by l_p) against both the external tension f and the side chain repulsive force f_{int}.

The additive tension model successfully describes the elasticity of the densely-grafted complex. We show fits of Eq. 2, using the same three-step methodology described above, in Fig. 3; the fit parameters are l_p, f_{int} and L_0. The fits result in acceptable goodness-of-fit metrics: $\bar{\chi}^2$ ranges from 1.5 to 2.5 across the five molecules tested. The best-fit persistence length is 2.1 ± 0.4 nm, and the best-fit internal tension is 1.3 ± 0.3 pN, each reported as mean $\pm$ standard deviation. The bare persistence length of unstacked ssDNA in the complete absence of electrostatic effects is ≈ 0.6 nm [21], significantly smaller than the value found from the fits here. We attribute the increased effective l_p to electrostatic stiffening, along with remnant stacking interactions that might be present, though the latter effect must be sufficiently weak to explain the lack of sigmoidal elastic response.

The measured internal tension, $f_{int} \approx 1.3$ pN, is consistent with estimates of the repulsive force between side chains. Using similar energetic-balance models as Birshtein *et al.* [6], Panyukov *et al.* [13] developed a scaling model that predicts:

$$f_{int} = \alpha k_B T b_s^{5/8} n^{3/8} \tau^{1/8} d^{-13/8}, \tag{3}$$

where d is the distance between the side chains and α is a numerical prefactor that is not fixed by the scaling model. We fix $\alpha = 1$, and estimate f_{int} using the side-chain parameters utilized above. We find d based on the range of relative extensions, $0.5 < L/L_0 < 0.92$, which indicates d ranges from $0.5 \times 6.1 = 3.1$ nm to $0.92 \times 6.1 = 5.6$ nm, given the contour length between grafting points of 6.1 nm. From Eq. 3, the estimated range of internal tensions is 1.2 pN $< f_{int} <$ 3.2 pN, consistent with the measured value.

In applying Eq. 2 to our single molecule data, a constant value of f_{int} is enforced over a range of polymer chain extensions, which contradicts the explicit dependence of f_{int} on extension through the parameter d in Eq. 3. This can be resolved by substituting Eq. 3 into Eq. 2; the resulting self-consistent expression for elasticity can then be fit to the data. Indeed, this approach more closely mirrors the Weiss molecular-field calculation, where the strength of the internal field is itself slaved to the magnetic polarization. However, we find that fitting the self-consistent expression gives nearly identical results as using a constant internal tension. This is likely because the form of the elasticity expression, Eq. 2, indicates that f_{int} will have minimal effect for $f \gg f_{int}$. Our data only minimally probe the $f \approx f_{int}$ regime; thus, while the experiment can detect the effect of internal tension, it lacks the resolution to determine if f_{int} varies with extension.

From a broad perspective, our results quantitatively demonstrate scale-dependent stiffness in a bottle-brush polymer. At the highest applied forces $f \gg f_{int}$, Eq. 2 indicates the chain will generate an entropic restoring force with a persistence length, $l_p \approx 2$ nm, due solely to main chain structure. As external force decreases, the internal tension begins to straighten the chain, increasing the effective persistence length. We estimate the force dependence of the effective persistence length, $l_{p,eff}(f)$, by forcing Eq. 2 to have the same form as Eq. 1, giving $l_{p,eff} \equiv l_p(1 + f_{int}/f)$. At the lowest applicable force, $f \approx f_{int}$, so the maximum effective stiffness is $l_{p,eff} \approx 2l_p = 4$ nm. This is roughly consistent with the low-force analysis: using the ideal-chain relation between Kuhn and persistence lengths, $b = 2l_p$, the low-

force Kuhn length is 8 nm. Keeping in mind that the scaling arguments we employ generally ignore numerical prefactors, this value is close to the estimate $b \approx 20$ nm made from analyzing the transitions out of the Pincus elastic regime.

In summary, we have demonstrated the utility of single-molecule elasticity measurements and the additive-tension elastic model in analyzing bottle brush structure. Our measurements specifically support the scaling estimates by Panyukov *et al.* [13] of the magnitude of the internal tension. We believe that the methodology and results demonstrated here will be useful in future studies of bottle brush behavior, including non-equilibrium dynamics of bottle-brush polymers in flow.

We acknowledge support from the National Science Foundation (O.A.S.: awards DMR 1309414 and DMR 1611497; C.M.S.: award CBET 1254340), and from the Camille & Henry Dreyfus Foundation (C.M.S.).

* saleh@engineering.ucsb.edu

[1] T. A. Waigh and A. Papagiannopoulos, Polymers **2**, 57 (2010).
[2] J. Montreuil, Pure and applied Chemistry **42**, 431 (1975).
[3] B. Button, L.-H. Cai, C. Ehre, M. Kesimer, D. B. Hill, J. K. Sheehan, R. C. Boucher, and M. Rubinstein, Science **337**, 937 (2012).
[4] J. J. Barr, R. Auro, M. Furlan, K. L. Whiteson, M. L. Erb, J. Pogliano, A. Stotland, R. Wolkowicz, A. S. Cutting, K. S. Doran, P. Salamon, M. Youle, and F. Rohwer, Proceedings of the National Academy of Sciences of the United States of America **110**, 10771 (2013).
[5] W. F. M. Daniel, J. Burdyńska, M. Vatankhah-Varnoosfaderani, K. Matyjaszewski, J. Paturej, M. Rubinstein, A. V. Dobrynin, and S. S. Sheiko, Nature Materials **15**, 183 (2016).
[6] T. Birshtein, O. Borisov, Y. B. Zhulina, A. Khokhlov, and T. Yurasova, Polymer Science USSR **29**, 1293 (1987).
[7] G. H. Fredrickson, Macromolecules **26**, 2825 (1993).
[8] J. Paturej, S. S. Sheiko, S. Panyukov, and M. Rubinstein, Science Advances **2** (2016).
[9] H.-P. Hsu, W. Paul, and K. Binder, Europhysics Letters **92**, 28003 (2010).
[10] J.-L. Barrat and J.-F. Joanny, Europhysics Letters (EPL) **24**, 333 (1993).
[11] H.-P. Hsu, W. Paul, and K. Binder, Macromolecules **43**, 3094 (2010).
[12] M. Ullner and C. E. Woodward, Macromolecules **35**, 1437 (2002).
[13] S. Panyukov, E. B. Zhulina, S. S. Sheiko, G. C. Randall, J. Brock, and M. Rubinstein, The Journal of Physical Chemistry B **113**, 3750 (2009).
[14] C. Brockman, S. J. Kim, and C. M. Schroeder, Soft Matter **7**, 8005 (2011).
[15] D. B. McIntosh, G. Duggan, Q. Gouil, and O. A. Saleh, Biophysical Journal **106**, 659 (2014).
[16] D. J. Mai, A. B. Marciel, C. E. Sing, and C. M. Schroeder, ACS Macro Letters **4**, 446 (2015).
[17] A. B. Marciel, D. J. Mai, and C. M. Schroeder, Macromolecules **48**, 1296 (2015).
[18] B. M. Lansdorp and O. A. Saleh, Review of Scientific Instruments **83**, 25110 (2012).
[19] N. Ribeck and O. A. Saleh, Review of Scientific Instruments **79**, 94301 (2008).
[20] K. Devanand and J. Selser, Macromolecules **24**, 5943 (1991).
[21] O. A. Saleh, D. B. McIntosh, P. Pincus, and N. Ribeck, Physical Review Letters **102**, 068301 (2009).
[22] P. Pincus, Macromolecules **9**, 386 (1976).
[23] R. R. Netz, Macromolecules **34**, 7522 (2001).
[24] O. A. Saleh, The Journal of Chemical Physics **142**, 194902 (2015).
[25] C. Ke, M. Humeniuk, H. S-Gracz, and P. E. Marszalek, Physical Review Letters **99**, 018302 (2007).
[26] J. F. Marko and E. D. Siggia, Macromolecules **28**, 8759 (1995).
[27] D. R. Jacobson, D. B. McIntosh, and O. A. Saleh, Biophysical Journal **105**, 2569 (2013).
[28] A. V. Dobrynin, J.-M. Y. Carrillo, and M. Rubinstein, Macromolecules **43**, 9181 (2010).
[29] D. R. Jacobson, D. B. McIntosh, M. J. Stevens, M. Rubinstein, and O. A. Saleh, Proceedings of the National Academy of Sciences **114**, 5095 (2017).
[30] P. Weiss, Journal de Physique Théorique et Appliquée **6**, 661 (1907).
[31] T. R. Strick, J.-F. Allemand, D. Bensimon, and V. Croquette, Biophysical Journal **74**, 2016 (1998).